Journal of Materials Chemistry C

ROYAL SOCIETY OF CHEMISTRY

PAPER

View Article Online
View Journal | View Issue

Cite this: J. Mater. Chem. C, 2023, 11, 11912

Magnetic carbon gate electrodes for the development of electrolyte-gated organic field effect transistor bio-sensing platforms†

Adrián Tamayo,[a] Jose Muñoz,‡[a] Carme Martínez-Domingo [a] and Marta Mas-Torrent *[ab]

Received 11th May 2023,
Accepted 7th August 2023

DOI: 10.1039/d3tc01655b

rsc.li/materials-c

Electrolyte-gated organic field-effect transistors (EGOFETs) are promising devices for the development of bio-sensors. Typically, a gold gate electrode is functionalised with a self-assembled monolayer bearing the bio-receptor. Here, we propose a new route to fabricate EGOFET sensors using magnetic carbon-paste gate electrodes. In this way, magnetic nanoparticles properly modified with a bio-receptor are incubated with the analyte and, subsequently, collected on the gate electrode surface. Remarkably, these electrodes can be polished and re-used after each measurement. The feasibility of this route is here demonstrated for the biotin–avidin/streptavidin supramolecular complexes. High sensitivities and low limits of detection of the order of fM are achieved. Hence, this work demonstrates a novel and versatile strategy to exploit EGOFETs as sensing platforms.

1. Introduction

Electrolyte-gated organic field effect transistors (EGOFETs) are raising a great deal of interest for the development of low-power electronic devices (*i.e.*, <1 V). EGOFET architecture consists of replacing the conventional dielectric layer of an organic field-effect transistor with an electrolyte, which is in direct contact with the organic semiconductor (OSC). In the last few years, these devices have also attracted considerable attention as electronic transducers in bio-sensing by using aqueous electrolytes.[1–8] Further, these organic-based devices are biocompatible and can be fabricated on flexible substrates using printing techniques. Thanks to these unique features, EGOFETs provide both an excellent interface between electronics and biology and the possibility to fabricate low cost disposable devices.[9,10] EGOFETs have already been reported to be appealing in applications such as medical diagnosis and cell activity recording.[11–15]

The operation mechanism of these devices relies on the formation of two electrical double layers (EDLs) at the OSC-electrolyte and electrolyte-gate interfaces upon the application of a gate voltage, which are responsible for the electrical tuning of the OSC.[16] Therefore, EGOFETs are highly sensitive to events occurring at the above-mentioned interfaces, which have been exploited for the development of bio-sensors by introducing suitable recognition groups.[5,17–19] For this purpose, the most employed approach has been focused on the chemical immobilisation of bio-receptors at the gate electrode using self-assembled monolayers (SAMs).[2,20–25] However, this methodology presents serious limitations since imperfections in the SAM might have important detrimental effects on the sensor response. Further, the long-term stability of SAMs and the limited number of active sites are also important drawbacks. Thus, there is a clear need to search for alternative routes that can widen the perspectives of EGOFETs as sensing platform.

Nanocomposite carbon paste-based electrodes have been extensively employed in electrochemistry due to the fact that they are biocompatible, and environmentally friendly, they show a stable response in aqueous media, and they have a high specific surface area and renewable surface.[26–29] Singularly, the fabrication of these electrodes allows for the easy incorporation of a magnet.[30] This has previously been exploited to trap magnetic nanoparticles (MNPs) with anchored bio-receptors to develop electrochemical sensors.[31–33] In these systems, the receptor–analyte interaction occurs in a MNPs suspension and, subsequently, the MNPs are collected with the electrode containing the magnet and the sensing response is electrochemically analysed. Interestingly, carbon paste-based electrodes have also been recently successfully applied as gate terminals in EGOFETs.[34,35] However, the use of such

[a] Institut de Ciència de Materials de Barcelona (ICMAB-CSIC), Campus de la UAB, 08193 Bellaterra, Spain. E-mail: mmas@icmab.es
[b] Networking Research Center on Bioengineering Biomaterials and Nanomedicine (CIBER-BBN) Campus de la UAB, 08193 Bellaterra, Spain

† Electronic supplementary information (ESI) available. See DOI: https://doi.org/10.1039/d3tc01655b

‡ Current address: Chemistry Department, Universitat Autònoma de Barcelona, 08193 Bellaterra, Spain.

carbon-gate electrodes combined with MNPs to develop EGOFET-based sensors has never been explored before. This approach could represent a rapid and cost-effective alternative to the conventional method employing SAMs for the development of sensitive EGOFET sensors.

In this work, we demonstrate the versatility of magnetic carbon-paste gate electrodes (CGE) as bio-sensing element in EGOFETs, employing as model recognition systems biotin–avidin (AV) and biotin–streptavidin (ST) complexes. The reported strategy provides clear advantages: (i) a high surface area for the receptor–analyte interaction, diminishing the required diffusion analyte distance, (ii) feasibility to concentrate the MNPs at the gate surface and (iii) possibility to re-use the electrodes. Remarkably, a high sensitivity for the detection of ST and AV equal to 0.07 ± 0.01 M^{-1} and 0.04 ± 0.02 M^{-1}, respectively, as well as a low limit of detection in the fM range was achieved. Thus, this work provides a novel promising route to apply EGOFETs in sensing.

2. Results

The EGOFET architecture employed in this work is shown in Fig. 1a. Thin films of the benchmark OSC 2,8-difluoro-5,11-bis(triethylsilylethynyl) anthradithiophene (diF-TES-ADT) blended with polystyrene (PS) (Fig. 1b) in a ratio 4 : 1 were deposited by Bar-Assisted Meniscus Shearing (BAMS) technique at 10 mm s^{-1} and 105 °C, as previously reported, on Kapton substrates with pre-fabricated Au source/drain interdigitated electrodes.[19,34,36,37] The CGE consisted in conductive reduced graphene oxide (rGO) dispersed within an insulating epoxy resin nanocomposite. The electrodes were mounted in a polyvinyl chloride (PVC) tube endowed with a magnet (see Experimental section and Fig. 1c).

As a first demonstration of applicability, the model complex biotin–streptavidin (ST) was explored, since it is one of the strongest non-covalent complexes. The strategy followed consisted in using cobalt iron oxide nanoparticles decorated with

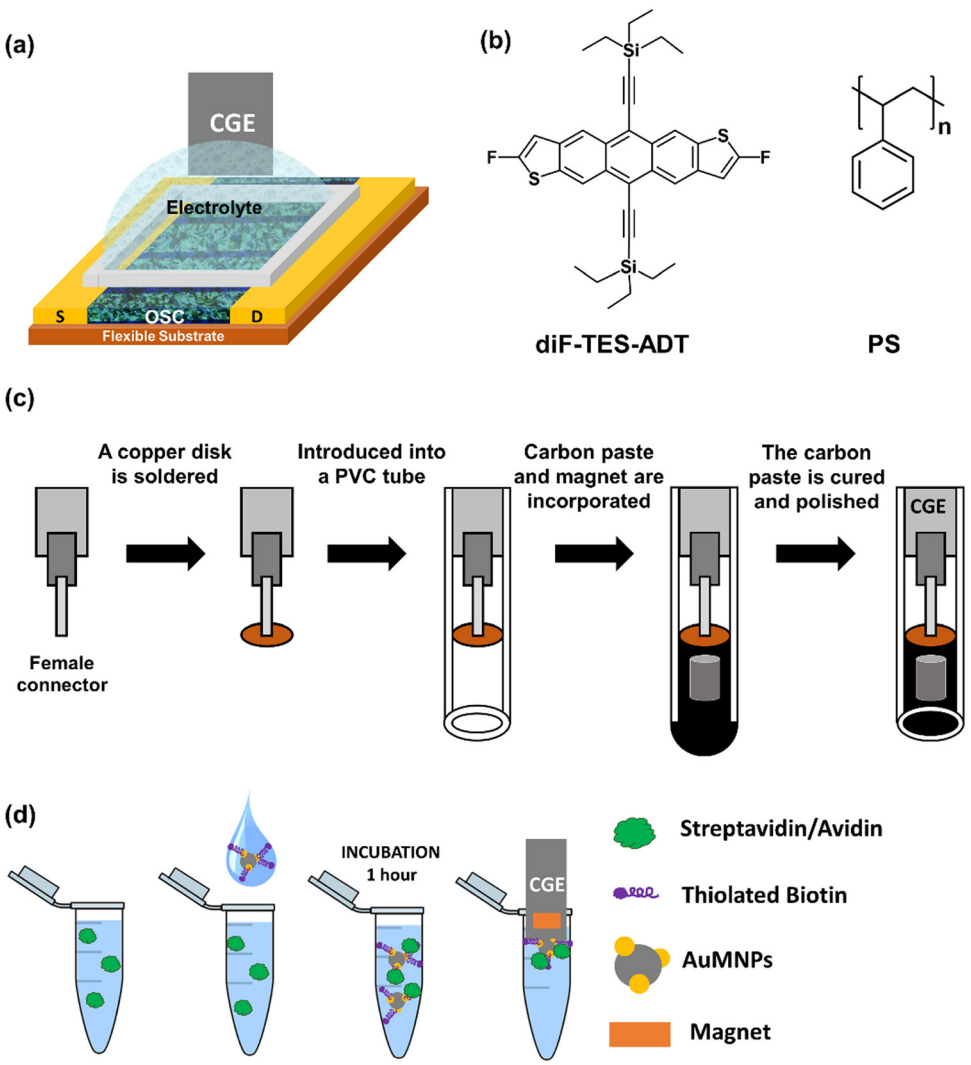

Fig. 1 (a) Scheme of the EGOFET structure. (b) Molecular structure of diF-TES-ADT and PS. (c) Schematic illustration of magnetic CGE fabrication. (d) Scheme of the sensing protocol.

Au nanoparticles (AuMNPs), which were subsequently functionalised with thiolated biotin (biotin-AuMNPs) adapting methods from literature[30,38] (see Experimental section).

The bare MNPs, AuMNPs and biotin-AuMNPs were analysed by different means. Transmission electron microscopy (TEM) and dynamic light scattering (DLS) characterisation indicated that the MNPs aggregation diminishes once they are decorated with Au and then, subsequently, with biotin (Fig. S1 and S2, ESI†). The presence of Au and biotin was supported by energy dispersive spectroscopy (EDX) data (Fig. S3, ESI†). Additionally, thermogravimetric analysis (TGA) measurements determined the organic load in the biotin-AuMNPs. The mass-loss profiles displayed two drops in weight equal to 3.6% between 100–200 °C and 15.5% between 250–450 °C compared to bare MNPs, which is attributed to the adsorbed water[39] and biotin[40] decomposition, respectively (Fig. S4, ESI†).

By performing electrochemical impedance spectroscopy (EIS) and cyclic voltammetry (CV) in a 0.1 M KCl solution containing 10 mM $[Fe(CN)_6]^{3-/4-}$ as redox probe, the ability of the biotin-AuMNPs to interact with ST was explored. This was performed by incubating the biotin-AuMNPs in a phosphate-buffered saline (PBS) solution with a concentration of 10^{-10} M of ST, and magnetically collecting them on a CGE surface (see Experimental section). CVs were acquired using as working electrode: (1) the bare CGE, and the CGE with collected (2) AuMNPs, (3) biotin-AuMNPs and (4) ST/biotin-AuMNPs (Fig. 2a). A gradual decrease in the anodic and cation peak current and an increment in the ΔE_p (peak-to-peak distance) were observed. This means that the charge transfer process is hindered with the increasingly modification of the MNPs. The impedance measurements also support this interpretation. A significant increase of the charge transfer resistance, R_{CT}, was observed after collecting the AuMNPs owing to the lower conductivity of the magnetic beads (Fig. 2b).[30] R_{CT} further increased progressively with the addition of, first, biotin, and then after the interaction with ST. Therefore, these results encouraged the implementation of the magnetic CGE as bio-recognition gate electrode in EGOFETs.

Prior to the sensing measurements, the electrical response of the EGOFET in ultrapure water (18.2 MΩ cm and pH = 7.6) was conditioned until reaching a steady-state current by applying a drain-source voltage (V_{DS}) and gate-source voltage (V_{GS}) equal to −0.4 V for 30–60 min. In parallel, a fixed concentration of biotin-AuMNPs were incubated for 60 minutes at room temperature under gentle stirring in 0.1 M PBS solutions containing ST in a concentration ranging from 0.6 fM to 0.6 nM (Fig. 1d). Subsequently, the ST/biotin-AuMNPs were magnetically collected on the CGE surface by immersing the electrode into the solution (Fig. S5, ESI†). Immediately afterwards, the CGE was implemented as gate electrode in the EGOFET. After each measurement of a specific ST concentration, the CGE was polished and re-used for the next experiment. Notice that blank reference transfer characteristics were recorded after each measurement to verify the re-usability of the CGEs and that the polishing of the electrode does not alter the electrical features of the transducer (see Fig. 3d and Fig. S6, ESI†).

As evidenced in Fig. 3a, increasing the ST concentration on the biotin-AuMNPs surface leads to a current increase in the transfer characteristics associated to a threshold voltage (V_{TH}) shift towards positive voltages (Fig. S7, ESI†). The rationale behind this behaviour is the binding of negatively charged species to the gate that act as an extra negative gating voltage. In such a scenario, a lower gate voltage is required to induce holes in the transistor channel. Indeed, by plotting the transfer characteristics as a function of $(V_{GS} - V_{TH})$, we can observe that the curves perfectly overlap (Fig. 3b). This is in agreement with

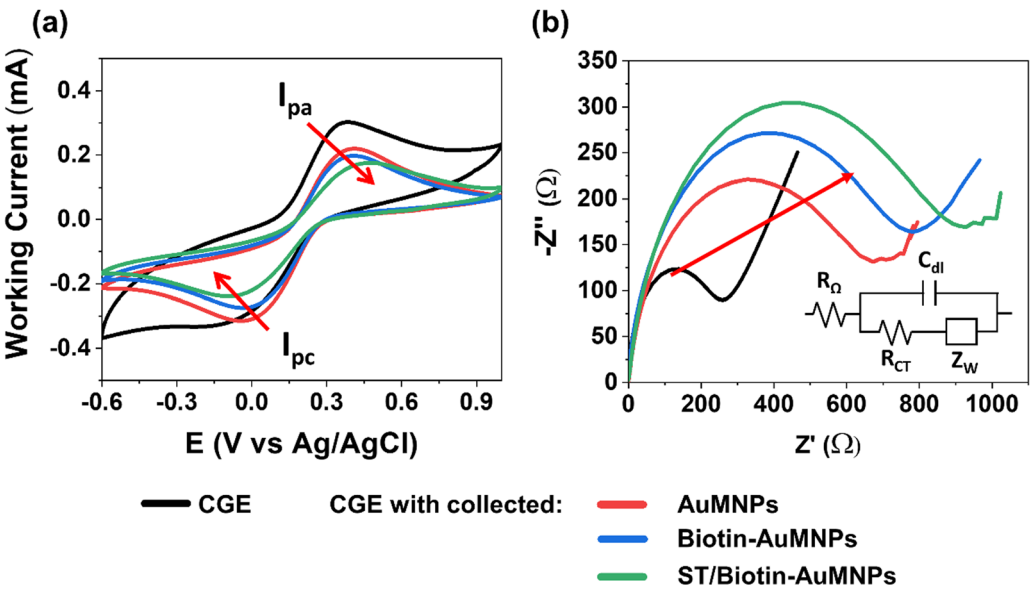

Fig. 2 (a) Cyclic voltammetry and (b) Nyquist plots for bare CGE, CGE with collected AuMNPs, CGE with collected biotin-AuMNPs and CGE with collected ST/biotin-AuMNPs ([ST] = 10^{-10} M). All the electrochemical measurements were carried out in a three-electrode configuration using a 0.1 M KCl aqueous solution containing 10 mM $[Fe(CN)_6]^{3-/4-}$ as redox probe.

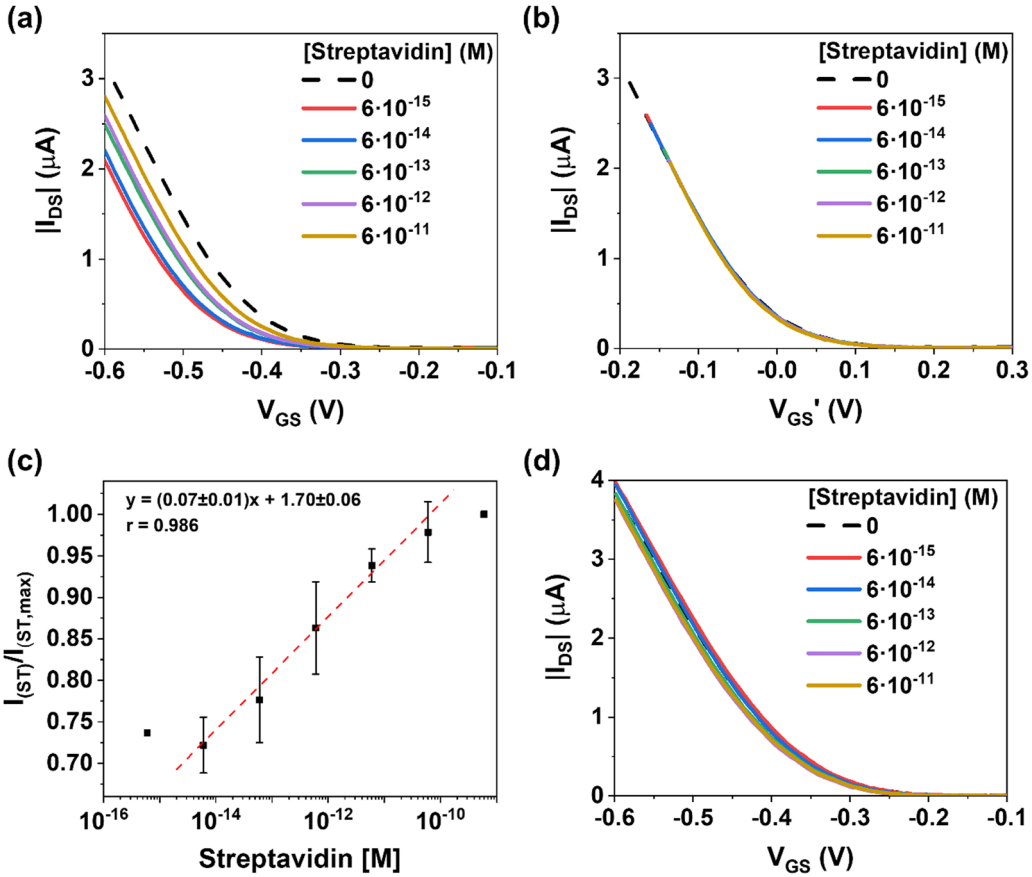

Fig. 3 (a) Transfer characteristics (V_{DS} = −0.1 V) of an EGOFET employing as gate electrode a CGE with collected biotin-AuMNPs previously incubated in a PBS solution with different ST concentrations. The dashed curve represents the transfer after the exposition to pure PBS solution. It should be noticed that the initial negative shift of the transfer characteristics upon exposition to ST could be caused by its effect on the nanoparticles dispersion. (b) Transfer characteristics shown in (a) as a function of the effective gate voltage ($V_{GS}' = V_{GS} - V_{TH}$). (c) Relative I_{DS} (at V_{GS} = −0.6 V) *vs.* ST concentration calibration. The bar error is relative to three different devices. (d) Transfer characteristic (V_{DS} = −0.1 V) of an EGOFET with a CGE gate electrode with collected MNPs incubated at different ST concentrations.

the fact that the binding of the analyte has a potentiometric effect on the EGOFET and the charge carrier mobility is clearly not affected.

The calibration curve was plotted for determining the sensitivity of the EGOFET evaluating the relative changes in the drain-source current (I_{DS}) at V_{GS} = −0.6 V (Fig. 3c). For each concentration, the average value and standard error are reported for 3 different devices. Remarkably, the EGOFET presents a wide operational range for [ST] over 4 orders of magnitude with a sensitivity of 0.07 ± 0.01 M^{-1} (r^2 = 0.98). Thus, our EGOFET permits to detect ST in the 6 fM-60 pM range. At ST concentration 0.6 nM, the EGOFET response shows a plateau indicating the saturation response of the CGE.

Aiming at excluding extrinsic phenomena (such as bias-stress or damaging of the semiconducting film) in the sensing performances, control *I–V* transfer characteristics were performed by using an EGOFET with a CGE gate electrode with collected MNPs bearing no biotin. As observed in Fig. 3d, no significant differences were noticed in the EGOFET electrical characteristics when solutions with varying ST concentrations were tested, indicating, thus, that the EGOFET changes previously observed were solely due to the biotin-ST interaction.

Charged proteins at the gate electrode have been experimentally shown to strongly affect the EGOFET response. As analytical models support, their net charge changes the surface potential, which modulates the channel current *via* the field effect.[17,18] The net charge of a protein depends on its structure and pH.[41] Biotin is known to form a strong supramolecular complex with ST and also with AV. Considering that the isoelectric point (IP) of ST is 6.1–7.5, whereas AV's IP is >10.5,[42,43] the electrical response of the EGOFET at pH 7–8 is expected to be opposite with the binding of these two analytes. Hence, we proceed to investigate the EGOFET response to the biotin–AV complex formation employing the same methodology.

Fig. 4a shows the dose–response of the EGOFET transfer characteristics. As expected, the positive charged analytes produce a current decrease ruled by a negative V_{TH} shift in the transfer characteristics. On the contrary to ST, accumulation of positive charges at the gate terminal renders lower effective gate voltages for the charge accumulation of the p-type semiconductor. By plotting the changes in current (V_{GS} = −0.6 V) as

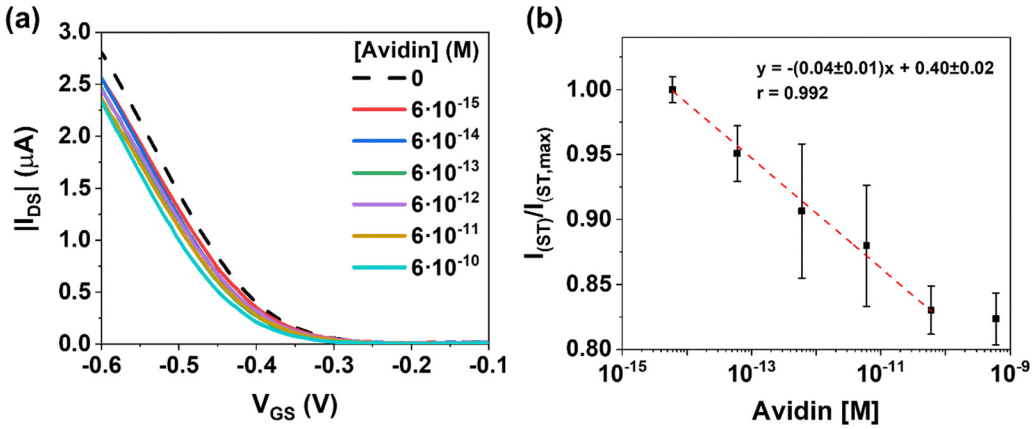

Fig. 4 (a) Transfer characteristics (V_{DS} = −0.1 V) of an EGOFET employing as gate electrode a CGE with collected biotin-AuMNPs previously incubated in a PBS solution of different AV concentrations. The dashed curve represents the transfer after the exposition of the CGE with collected biotin-AuMNPs to a reference PBS solution. (b) Relative I_{DS} (at V_{GS} = −0.6 V) *vs.* AV concentration plot and the calibration.

function of AV concentration in the range 6 fM to 0.6 nM (Fig. 4b), a sensitivity of (0.04 ± 0.01) M^{-1} was extracted. Similar to the ST case, at concentration 0.6 nM of AV, the sensor saturated. As in the previous case, the control experiment using bare MNPs did not respond to the presence of AV (Fig. S8, ESI†). Comparable responses in the dynamic range are acquired for ST and AV; whereas ST stands for a current change of nearly +30%, the AV shows a drop of −20%.

A number of works have reported on the potential utilization of biotin–AV/ST interaction in sensing technologies. Employing diverse detection methods, such as competitive immunoassay, electrochemical or field-effect transistors, detection limits ranging from 10 fM to ∼90 nM have been reported (Table S1, ESI†).[4,44–52] Hence, considering all this, it is clear that the EGOFET biosensor technology here reported shows a very high sensitivity and, in addition, has the advantage of using low-cost manufacturing procedures and an easily readable electrical signal. Avidin-biotin systems are being used to detect a wide variety of analytes through the biotinylation. Similarly, the present EGOFET is expected to be employed for the detection of antigen–antibody, nucleic acid systems and other bioactive macromolecules. The potential of the present work is the combination of the ultra-sensitive detection of EGOFETs[5,10,14,15,25,53] with the fabrication of cheap and reusable CGE for developing point-of-care sensors.

3. Conclusions

Overall, the approach of magnetically collecting functionalised magnetic nanoparticles on electrodes, which has been employed in the past for the development of electrochemical biosensors, has been here extended in EGOFETs. Thus, gate electrodes based on magnetic carbon-paste electrodes have been employed as alternative to the conventional gold-functionalised gate contacts used in EGOFET sensors. Remarkably, these carbon-paste electrodes can be polished and re-used after each measurement. As a proof of concept, biotin-modified AuMNPs were used to detect streptavidin and avidin. In both cases, high sensitivities and low limits of detection of the order of fM have been achieved, elucidating the potential of this strategy and opening new avenues for the application of EGOFETs as sensing platform.

4. Experimental

4.1. Chemicals and reagents

2,8-Difluoro-5,11-bis(triethylsilylethynyl)anthradithiophene (diF-TES-ADT, 99%) was purchased from Lumtec and used without further purification. Polystyrene (PS, $M_W \approx 10000$ g mol^{-1}), 2,3,4,5,6-pentafluorothiophenol (PFBT, 97%), anhydrous chlorobenzene (≥99.5%), streptavidin from streptomyces avidin (affinity purified, lyophilized from 10 mM potassium phosphate, ≥13 U per mg protein), avidin from egg white (BioUltra, lyophilized powder, ≥10 units per mg protein), graphene oxide (GO) powder and cobalt iron oxide nanopowder (30 nm particle size) were purchased from Sigma Aldrich and used without further purification. The HS–$(CH_2)_{11}$–NH–C(O)–biotin, refereed as thiolated biotin, was purchased from ProChimia Surfaces Sp and used without further purification. The Epotek H77 polymeric matrix was obtained from Epoxy Technology (Billerica, MA, USA). Kapton® substrates (Kapton®HN, 75 μm thick) used for the transistors were purchased from DuPont (Wilmington, DE, USA). All organic solvents were of HPLC grade. Ultrapure water (18.2 MΩ cm) was obtained from a Milli-Q system (Millipore, Billerica, MA, USA).

4.2. Synthesis of the nanoparticles

Synthesis of gold decorated cobalt ferrite nanoparticles (AuMNPs): Cobalt iron oxide nanoparticles were dispersed in ultrapure water (1.5 mg mL^{-1}, 50 mL), ultrasonicated for 1 h and stirred for 30 min at room temperature. An equal volume of $HAuCl_4$ (5 mM) was added to the suspension, which was then stirred for 30 min more. $HAuCl_4$ was reduced onto the $CoFe_2O_4$ MNPs surface[54,55] by adding 100 mL of $NaBH_4$ solution (0.1 M),

as previously reported.[30] Finally, the AuMNPs were extracted magnetically and washed several times with ultrapure water. Afterwards, AuMNPs were immersed in a solution of thiolated biotin (0.1 mM in ultrapure water) for 24 h. Next, the biotin-AuMNPs were extracted magnetically and, washed several times with ultrapure water.

Microscopy images of AuMNPs and the EDX measurements were obtained by High Resolution Transmission Electron Microscopy (HR–TEM) unit with an acceleration voltage of 120 kV and energy-dispersive detector. Dynamic Light Scattering (DLS) measurements were carried out by a Zetasizer Nano ZS using a plastic micro cuvette from Malvern Panalytical. The samples (1 mL) were analyzed without any previous modification and diluted in a ratio of 1 : 10. Thermal stability measurements of, biotin-AuMNPs and MNPs were carried out by thermal gravimetric analysis (TGA) in a range temperature among 25–500 °C with a heating rate of 10 °C min^{-1} under air atmosphere by the NETZSCH -STA 449 F1 Jupiter equipment.

4.3. CGE fabrication

A copper disk (5 mm of diameter and 1 mm of thickness) was soldered to a female connector (2 mm of diameter) and then introduced into a polyvinylchloride (PVC) tube (6 mm of internal diameter and 20 mm of length) as depicted in Fig. 1c. Then, reduced graphene oxide (rGO) was synthesized from graphene oxide (GO) *via* ascorbic acid reduction.[56,57] The GO dispersed in deionized water (1.5 mg mL^{-1}) was firstly ultrasonicated for 1 h, and then stirred for 30 min at room temperature. Finally, the GO was reduced using ascorbic acid (1 mM) to obtain the conducting reduced graphene oxide (rGO). The carbon paste of the CGEs were fabricated by dispersing the rGO (13 wt%) within an Epotek H77 epoxy resin (87 wt%) through manually homogenization for 60 min.[34]

Lastly, the PVC tubes were filled with the nanocomposite paste to form the body of the CGE electrode, where a neodymium magnet (3 mm diameter and 3 mm height) was embedded. Afterwards, the electrodes were cured at 80 °C for 24 h. Finally, the resulting CGEs were polished with different sandpapers of decreasing grain size (800 and 1200) until obtaining a totally flat surface. The resultant geometric area of the CGE was 28 mm^2.

4.4. EGOFET fabrication

Source/drain electrodes were defined on Kapton foil (Kapton® HN from DuPont, 75 μm thick) by photolithography (MicroWriter ML™ Laser Lithography System). Metal interdigitated electrodes of Cr/Au (5 nm/40 nm) were deposited by thermal evaporation (System Auto 360 from BOC Edwards). The channel width (W) and length (L) were 5000 μm and 50 μm (W/L = 100), respectively. Before the deposition of the active layer, the substrates were cleaned in ultrasonic bath with acetone and isopropanol and then dried under nitrogen flow. The gold electrodes were chemically modified with PFBT. For this purpose, the substrates were first exposed to ultraviolet ozone for 25 min and then immersed in a PFBT solution (15 mM) in isopropanol for 15 min. 2 wt% solutions of diF-TES-ADT and PS in chlorobenzene were mixed in 4 : 1 volume ratio, respectively. The resulting solution was deposited on the Kapton substrate containing the electrodes using the BAMS technique at a coating speed of 10 mm s^{-1} and at 105 °C, as previously reported.[36]

4.5. Electrical and electrochemical characterisation

4.5.1. Electrochemical characterization. Electrochemical characterizations by means of cyclic voltammetry (CV) and electrochemical impedance spectroscopy (EIS) were performed using AutoLab Metrohm PGSTAT128N potentiostat/galvanostat equipped with NOVA 2.1.3 software. CV and EIS experiments were carried out using a three-electrode configuration cell using as electrolyte 20 mL of 0.1 M KCl aqueous solution containing 10 mM of $[Fe(CN)_6]^{3-/4-}$ as redox marker. A single junction reference electrode Ag/AgCl (3 M) and a platinum wire were used as reference and auxiliary electrodes, respectively. The developed CGEs were employed as working electrodes.

EIS measurements were obtained by applying a sine wave with amplitude of 5 mV and a redox equilibrium potential of 150 mV over the frequency range from 100 kHz to 0.1 Hz (equilibrium time: 10 s).

4.5.2. Electrical characterization of the EGOFETs. Electrical characteristics of the EGOFETs were obtained using an Agilent 1500 A semiconductor analyser equipment connected to the samples through of a SÜSS probe station. The transfer and output characteristics were performed by confining 200–300 μL of ultrapure water over of the active area with a PDMS well. All the measurements were carried out in ambient and dark conditions.

The EGOFETs were electrically stabilized by means of transfer characteristics for 30–60 minutes before performing the sensing measurements. Transfer characteristics were recorded in lineal (V_{DS} = −0.10 V) regime. Eqn (1) expresses the drain current in lineal regime, where μ is the charge-carrier field-effect mobility ($cm^2\ V^{-1}\ s^{-1}$) and C is the electrical double layer capacitance per unit area (estimated value of C = 5.3 μF cm^{-2} as previously reported).[36]

$$I_{DS} = \mu C \frac{W}{L}(V_{GS} - V_{TH})V_{DS} \quad (1)$$

4.5.3. Sensing measurements. Before each electrical measurement, the surface of the CGE was polished, and then it was then rinsed with ultrapure water to remove any polishing residues.

The incubation protocols consisted of the following steps:

(i) The 200 μL of biotin-AuMNPs solution at 1 mg mL^{-1} were incubated for 1 hour at room temperature under gentle stirring (by Heidolph Inkubator 1000) in 300 μL of 0.1× phosphate-buffered saline (PBS) solutions containing ST (or AV) from low (fM) to high concentrations (nM) in order to minimize the accumulation error.

(ii) Then, incubated biotin-AuMNPs were magnetically collected on the CGE surface by immersing the electrode into the solution and rinsing with ultrapure water.

(iii) Afterwards the electrodes were electrically analysed in the EGOFET.

(iv) After the electrical measurements, the CGE was polished and re-used.

(v) The same protocol was then used with MNPs as control to verify that the electrical characteristics of the CGE were preserved.

Conflicts of interest

There are no conflicts to declare.

Acknowledgements

This work was funded by the Spanish Government within the research project GENESIS PID2019-111682RB-I00 and the ''Severo Ochoa'' Programme for Centers of Excellence in R&D (FUNFUTURE CEX2019-000917-S). Funding was also provided by the Generalitat de Catalunya (2021 SGR 00443). C. M. acknowledges the Juan de la Cierva fellowship.

References

1 D. Wang, V. Noël and B. Piro, *Electronics*, 2016, **5**, 9.
2 S. Casalini, A. C. Dumitru, F. Leonardi, C. A. Bortolotti, E. T. Herruzo, A. Campana, R. F. De Oliveira, T. Cramer, R. Garcia and F. Biscarini, *ACS Nano*, 2015, **9**, 5051–5062.
3 M. Berto, S. Casalini, M. Di Lauro, S. L. Marasso, M. Cocuzza, D. Perrone, M. Pinti, A. Cossarizza, C. F. Pirri, D. T. Simon, M. Berggren, F. Zerbetto, C. A. Bortolotti and F. Biscarini, *Anal. Chem.*, 2016, **88**, 12330–12338.
4 G. Palazzo, D. De Tullio, M. Magliulo, A. Mallardi, F. Intranuovo, M. Y. Mulla, P. Favia, I. Vikholm-Lundin and L. Torsi, *Adv. Mater.*, 2015, **27**, 911–916.
5 E. Macchia, K. Manoli, B. Holzer, C. Di Franco, M. Ghittorelli, F. Torricelli, D. Alberga, G. F. Mangiatordi, G. Palazzo, G. Scamarcio and L. Torsi, *Nat. Commun.*, 2018, **9**, 3223.
6 F. Torricelli, D. Z. Adrahtas, Z. Bao, M. Berggren, F. Biscarini, A. Bonfiglio, C. A. Bortolotti, C. D. Frisbie, E. Macchia, G. G. Malliaras, I. Mcculloch, M. Moser, T.-Q. Nguyen, R. M. Owens, A. Salleo, A. Spanu and L. Torsi, *Nat. Rev. Methods Primers*, 2021, **1**, 66.
7 K. Solodka, M. Berto, D. Ferraro, C. Menozzi, M. Borsari, C. A. Bortolotti, F. Biscarini and M. Pinti, *Adv. Mater. Interfaces*, 2022, **9**, 2102341.
8 J. Tong, A. Doumbia, R. U. Khan, A. Rahmanudin, M. L. Turner and C. Casiraghi, *Nano Lett.*, 2022, **22**, 2643–2649.
9 L. Kergoat, B. Piro, M. Berggren, G. Horowitz and M. C. Pham, *Anal. Bioanal. Chem.*, 2012, **402**, 1813–1826.
10 P. Seshadri, K. Manoli, N. Schneiderhan-Marra, U. Anthes, P. Wierzchowiec, K. Bonrad, C. Di Franco and L. Torsi, *Biosens. Bioelectron.*, 2018, **104**, 113–119.
11 R. Furlan de Oliveira, V. Montes-García, P. A. Livio, M. B. González-García, P. Fanjul-Bolado, S. Casalini and P. Samorì, *Small*, 2022, **18**, 2201861.
12 A. Kyndiah, F. Leonardi, C. Tarantino, T. Cramer, R. Millan-Solsona, E. Garreta, N. Montserrat, M. Mas-Torrent and G. Gomila, *Biosens. Bioelectron.*, 2020, **150**, 111844.
13 K. Schmoltner, J. Kofler, A. Klug and E. J. W. List-Kratochvil, *Org. Field Eff. Transistors XII, Org. Semicond. Sensors Bioelectron. VI*, 2013, **8831**, 88311N.
14 S. K. Sailapu, E. Macchia, I. Merino-Jimenez, J. P. Esquivel, L. Sarcina, G. Scamarcio, S. D. Minteer, L. Torsi and N. Sabaté, *Biosens. Bioelectron.*, 2020, **156**, 112103.
15 M. Selvaraj, P. Greco, M. Sensi, G. D. Saygin, N. Bellassai, R. D'Agata, G. Spoto and F. Biscarini, *Biosens. Bioelectron.*, 2021, **182**, 113144.
16 L. Kergoat, L. Herlogsson, D. Braga, B. Piro, M. C. Pham, X. Crispin, M. Berggren and G. Horowitz, *Adv. Mater.*, 2010, **22**, 2565–2569.
17 S. Casalini, F. Leonardi, T. Cramer and F. Biscarini, *Org. Electron.*, 2013, **14**, 156–163.
18 M. Magliulo, A. Mallardi, M. Y. Mulla, S. Cotrone, B. R. Pistillo, P. Favia, I. Vikholm-Lundin, G. Palazzo and L. Torsi, *Adv. Mater.*, 2013, **25**, 2090–2094.
19 S. Ricci, S. Casalini, V. Parkula, M. Selvaraj, G. D. Saygin, P. Greco, F. Biscarini and M. Mas-Torrent, *Biosens. Bioelectron.*, 2020, **167**, 112433.
20 I. M. Bhattacharyya, S. Cohen, A. Shalabny, M. Bashouti, B. Akavayov and G. Shalev, *Biosens. Bioelectron.*, 2019, **132**, 143–161.
21 E. Macchia, K. Manoli, B. Holzer, C. Di Franco, R. A. Picca, N. Cioffi, G. Scamarcio, G. Palazzo and L. Torsi, *Anal. Bioanal. Chem.*, 2019, **411**, 4899–4908.
22 A. Molazemhosseini, F. A. Viola, F. J. Berger, N. F. Zorn, J. Zaumseil and M. Caironi, *ACS Appl. Electron. Mater.*, 2021, **3**, 3106–3113.
23 C. Diacci, M. Berto, M. Di Lauro, E. Bianchini, M. Pinti, D. T. Simon, F. Biscarini and C. A. Bortolotti, *Biointerphases*, 2017, **12**, 05F401.
24 M. Berto, E. Vecchi, L. Baiamonte, C. Condò, M. Sensi, M. Di Lauro, M. Sola, A. De Stradis, F. Biscarini, A. Minafra and C. A. Bortolotti, *Sens. Actuators, B*, 2019, **281**, 150–156.
25 M. Berto, C. Diacci, R. D'Agata, M. Pinti, E. Bianchini, M. Di Lauro, S. Casalini, A. Cossarizza, M. Berggren, D. Simon, G. Spoto, F. Biscarini and C. A. Bortolotti, *Adv. Biosyst.*, 2018, **2**, 1700072.
26 J. Muñoz, R. Montes and M. Baeza, *TrAC, Trends Anal. Chem.*, 2017, **97**, 201–215.
27 M. Pumera, A. Merkoçi and S. Alegret, *Sens. Actuators, B*, 2006, **113**, 617–622.
28 I. Švancara, K. Vytřas, K. Kalcher, A. Walcarius and J. Wang, *Electroanalysis*, 2009, **21**, 7–28.
29 J. Muñoz and M. Baeza, *Electroanalysis*, 2017, **29**, 1660–1669.
30 J. Muñoz, A. González-Campo, M. Riba-Moliner, M. Baeza and M. Mas-Torrent, *Biosens. Bioelectron.*, 2018, **105**, 95–102.
31 M. Ahmadi, A. Ghoorchian, K. Dashtian, M. Kamalabadi, T. Madrakian and A. Afkhami, *Talanta*, 2021, **225**, 121974.
32 X. Deng, W. Li, Y. Wang and G. Ding, *TrAC, Trends Anal. Chem.*, 2020, **124**, 115804.

33 F. Mollarasouli, E. Zor, G. Ozcelikay and S. A. Ozkan, *Talanta*, 2021, **226**, 122108.
34 A. Tamayo, J. Muñoz and M. Mas-Torrent, *Adv. Electron. Mater.*, 2020, **6**, 2000431.
35 J. Muñoz, F. Leonardi, T. Özmen, M. Riba-Moliner, A. González-Campo, M. Baeza and M. Mas-Torrent, *J. Mater. Chem. C*, 2019, **7**, 14993–14998.
36 Q. Zhang, F. Leonardi, S. Casalini, I. Temiño and M. Mas-Torrent, *Sci. Rep.*, 2016, **6**, 39623.
37 Q. Zhang, A. Tamayo, F. Leonardi and M. Mas-Torrent, *ACS Appl. Mater. Interfaces*, 2021, **13**, 30902–30909.
38 N. Liu, X. Xiang, L. Fu, Q. Cao, R. Huang, H. Liu, G. Han and L. Wu, *Biosens. Bioelectron.*, 2021, **188**, 113340.
39 M. Ansari, M. Habibi-Rezaei, S. Salahshour-Kordestani, M. Ferdousi and A. A. M. Movehedi, *Mater. Technol.*, 2016, **31**, 315–321.
40 Q. Han, L. Huang, Q. Luo, Y. Wang, M. Wu, S. Sun, H. Zhang and Y. Wang, *RSC Adv.*, 2021, **11**, 18084–18092.
41 N. Haustein, Ó. Gutiérrez-Sanz and A. Tarasov, *ACS Sens.*, 2019, **4**, 874–882.
42 Y. Takakura, K. Sofuku, M. Tsunashima and S. Kuwata, *J. Biosci. Bioeng.*, 2016, **121**, 420–423.
43 L. Almonte, E. Lopez-Elvira and A. M. Baro, *Chem. Phys. Chem.*, 2014, **15**, 2768–2773.
44 W. Z. Lin, Y. H. Chen, C. K. Liang, C. C. Liu and S. Y. Hou, *Food Chem.*, 2019, **271**, 440–444.
45 S. J. Ding, B. W. Chang, C. C. Wu, M. F. Lai and H. C. Chang, *Electrochim. Acta*, 2005, **50**, 3660–3666.
46 N. Bage and P. Kar, *Sens. Int.*, 2022, **3**, 100159.
47 S. V. Kergaravat, G. A. Gómez, S. N. Fabiano, T. I. Laube Chávez, M. I. Pividori and S. R. Hernández, *Talanta*, 2012, **97**, 484–490.
48 A. Buzid, G. P. McGlacken, J. D. Glennon and J. H. T. Luong, *ACS Omega*, 2018, **3**, 7776–7782.
49 S. Wang, M. Z. Hossain, T. Han, K. Shinozuka, T. Suzuki, A. Kuwana and H. Kobayashi, *ACS Omega*, 2020, **5**, 30037–30046.
50 J. Lee, M. J. Kim, H. Yang, S. Kim, S. Yeom, G. Ryu, Y. Shin, O. Sul, J. K. Jeong and S. B. Lee, *IEEE Sens. J.*, 2021, **21**, 178–184.
51 H. Yang and T. Sakata, *Sensors*, 2019, **19**, 3393.
52 Z. S. Kim, S. C. Lim, S. H. Kim, Y. S. Yang and D. H. Hwang, *Sensors*, 2012, **12**, 11238–11248.
53 E. Y. Poimanova, P. A. Shaposhnik, D. S. Anisimov, E. G. Zavyalova, A. A. Trul, M. S. Skorotetcky, O. V. Borshchev, D. Z. Vinnitskiy, M. S. Polinskaya, V. B. Krylov, N. E. Nifantiev, E. V. Agina and S. A. Ponomarenko, *ACS Appl. Mater. Interfaces*, 2022, **14**, 16462–16476.
54 J. Muñoz, R. Montes, J. Bastos-Arrieta, M. Guardingo, F. Busqué, D. Ruíz-Molina, C. Palet, J. García-Orellana and M. Baeza, *Sens. Actuators, B*, 2018, **273**, 1807–1815.
55 J. Muñoz, J. Bastos-Arrieta, M. Muñoz, D. Muraviev, F. Céspedes and M. Baeza, *RSC Adv.*, 2014, **4**, 44517–44524.
56 J. Muñoz, L. J. Brennan, F. Céspedes, Y. K. Gun'ko and M. Baeza, *Compos. Sci. Technol.*, 2016, **125**, 71–79.
57 M. J. Fernández-Merino, L. Guardia, J. I. Paredes, S. Villar-Rodil, P. Solís-Fernández, A. Martínez-Alonso and J. M. D. Tascón, *J. Phys. Chem. C*, 2010, **114**, 6426–6432.